Experimental and numerical analysis of the energy efficiency of PCM concrete wallboards under different thermal scenarios

Nessrine Essid [a], Anissa Eddhahak [b,*], Jamel Neji [a]

[a] Tunis El Manar University, National Engineering School of Tunis; LR11ES16 Laboratory of Materials, Optimization, and Environment for Sustainability, B.P. 37 Le Belvédère, 1002 Tunis, Tunisia
[b] PIMM Laboratory, CNRS UMR 8006, Arts et Métiers ParisTech, 151 bd de l'Hôpital, 75013 Paris, France

Keywords:
PCM-Concrete
Wallboard
FEM simulation
Thermal scenarios
Energy efficiency

A B S T R A C T

This paper aims to investigate the energy efficiency of PCM-concrete wallboards using experimental and numerical approaches. First, a laboratory experimental work was performed to manufacture PCM-concrete mixtures with different proportions of PCMs. Then, an innovative bench test based on the transient plane source theory was used for the thermal analysis of the mixtures. Besides, numerical simulation by finite element method was carried and the confrontation of the numerical results with the experience has showed an excellent agreement. Accordingly, the numerical approach was validated and generalized for the study of PCM-concrete at macro scale under different thermal scenarios and PCM distributions (homogeneous/Bilayer/Matrix-inclusions). The numerical simulations highlighted clearly the role of PCMs in decreasing the indoor temperature of the different PCM-wallboards as well as the thermal fluctuations. Moreover, the time delay in the temperature peaks emphasized the enhancement of the energy efficiency of PCM-wallboards in comparison with a traditional concrete, especially for the case of the bilayer wallboard.

1. Introduction

According to the International Energy Agency, the energy consumption of buildings is expected to rise to about 50% in 2050 [1,2]. As a consequence, improving the thermal storage performance of the building envelope is essential for reducing air conditioning energy consumption and enhancing indoor thermal comfort [3,4]. In the recent years, some studies have considered the strategies of combining micro-encapsulated phase change materials PCMs with high latent heat, with civil engineering traditional materials, such as concrete to improve the thermal performance and the energy efficiency of the building [5–10]. In fact, PCMs have the advantage of absorbing large amounts of energy in a comparatively very small volume at a nearly constant temperature. Thus, PCMs integration in construction materials and especially in the building envelope can improve the thermal storage capacity of the building and ultimately contributes to keeping the inside temperature relatively constant with low variations [11,12].

Apart from the experimental extensive works in literature, many researches have focused on the investigation of PCMs energy efficiency from a numerical point of view [13–15]. Some numerical methods based on the statement of the heat transfer equations, have been proposed for modelling and solving the heat transfer phenomenon in presence of a phase change (solid-liquid) component. Among them, one can mention the approaches illustrated by the effective heat capacity, the additional heat source, and the enthalpy methods, for instance Ref. [16]. Other numerical approaches based generally on the finite element methods are particularly very attractive since they have the advantageous to simulate the PCM-material at macro scale, by considering different loading scenarios and geometric parameters, saving thereby a laborious experimental laboratory work.

For instance, this holds for the research of Xaman et al. (2019) [17] who studied the thermal performance of a concrete roof with a PCM layer placed under a Mexican warm weather (Merida). Three types of PCMs were considered: Paraffin wax - MG29 (R-PCM1), N-Eicosane (R-PCM2), and Salt Hydrates (R-PCM3) and different thickness values of the PCM layer were used. The numerical simulations were conducted during the warmest and the coldest days of the year. The results indicated that the case R-PCM1 with 2 cm of PCM layer had the lowest values of thermal load during the coldest and the warmest day. These values are up to 57% lower than the thermal load corresponding to the conventional concrete roof. Therefore, the authors concluded their study by recommending the R-PCM1 with 2 cm of PCM layer to improve the

thermal behavior of buildings.

On the other hand, Yu et al. (2019) [18] proposed a pipe-embedded ventilation roof with outer-layer shape-stabilized PCM. A three-dimensional transient-state heat transfer model was developed by CFD tools. Then, the authors evaluated the effects of phase change temperature range of PCMs as well as the thickness of PCM layer and airflow rate in the ventilation duct, on the thermal behavior of the building by considering five representative climate regions of China. The results of their study showed that the optimum phase transition temperature ranges of PCM are 31–33 °C, 34–36 °C, 36–38 °C, 34–36 °C and 29–31 °C, in severe cold region, cold region, hot summer and cold winter region, hot summer and warm winter region and mild region, respectively. The optimum thicknesses of the PCM layer were estimated to 25–30 mm, 25–30 mm, 30–35 mm, 25–30 mm and 20–25 mm, respectively.

Kheradmandet al. (2015) [19] studied the simultaneous incorporation of hybrid PCMs in plastering mortars for façade walls. The thermal performance of this technology was experimentally evaluated by comparing the behavior of a prototype test cell made with hybrid PCMs, with a reference prototype (without PCMs) under realistic daily temperature configuration. A numerical simulation model using the commercial software ANSYS-FLUENT was developed. Results showed that the incorporation of hybrid PCMs into plastering mortars significantly can reduce heating/cooling temperature demands for maintaining interior thermal comfort when compared to reference mortars and mortars with a single type of PCMs.

In this context, the present study is a contribution to further investigate the energy efficiency of commercial PCMs labelled “Micronal” [20], especially designed for the sector building uses. It shall be noted that this work is involved in the framework of a larger research dealing with the sustainable strategies assessed for the energy storage in smart buildings. Several studies of the authors dealing especially with the identification of the thermophysical properties of Micronal PCMs, and the evaluation of their performances when integrated into cement-based materials were previously published [21–26].

Drissi et al. [21] performed a laboratory thermal characterization of PCMs and Portland cement concretes embedded with PCMs using various experimental techniques. In their study, several PCM-concrete mixtures were manufactured with different amounts of PCMs, then the specific heat capacity was analysed by differential scanning calorimetry technique, whereas the thermal conductivity was measured by hot disk. The results highlighted an improvement of the heat storage capacity of the PCM-concrete with PCMs addition and a decrease of their thermal conductivity [23,26]. This finding was corroborated later by the research of Essid et al. [22] performed on both mortar and concrete cubic specimens embedded with PCMs.

Furthermore, given the importance of the processing conditions in governing the microstructure and therefore the macroscopic properties of the PCM-concrete, studies have been carried by the authors in order to optimise the manufacture of the cement-based materials incorporating PCMs. In a previous research by the authors [25], for instance, some capsules were intentionally subjected to damage in laboratory. Then, the thermal properties of damaged PCM-concrete mixes were investigated by DSC and compared to the reference PCM concrete. The obtained results highlighted a loss of the specific heat capacity by about 28% compared to the non-damaged PCMs.

Despite the numerous advantages of PCM from a thermal point of view, a major mechanical disadvantage related to the decrease of the compressive resistance of the construction material was emphasized. Accordingly, attention has been paid to the hydration kinetic of PCM-mortars embedded with damaged and non-damaged PCMs based on a modified semi-adiabatic calorimetry method [24]. The research highlighted a delay in the hydration progress with the addition of PCMs, which was more pronounced in the case of mortars with damaged capsules. Other investigations have been oriented towards the study of the hygric properties of the PCM-materials like porosity and permeability in relation with the PMCs addition, as highlighted in a previous paper of the authors [27].

In the continuity of the aforementioned researches performed at the material scale, this study aims to take advantages of the achieved works in order to study the Micronal PCM-concrete at macro scale. A preliminary experimental part of this study was performed on a PCM-concrete wallboard, with different PCMs ratios, by using an original bench test developed in laboratory. Then, a numerical finite element method was assessed and validated by comparison with the experience results. The extension of the numerical method to the case of a full-scale PCM-concrete was achieved under different climate conditions and PCMs distributions in the wallboard. The results were analysed and discussed for the different configurations and during the storage and release periods of PCMs.

2. Materials and methods

2.1. Phase change materials

The solid–liquid microencapsulated PCMs used in this study are commercial product named Micronal with a melting temperature of 25 °C and a latent heat capacity of 110 kJ kg^{-1} [20]. The used PCMs are dry powder of paraffin wax mixture encapsulated in a highly cross-linked polymer: the Polymethylmethacrylate (PMMA), free of formaldehyde. PCMs can be agglomerated together to form spherical microcapsules of 50–300 μm of diameter. The particle size distribution of PCMs is determined by the dry process in order to avoid any potential risk of interference of the polymer matrix of PCMs with water. The sieve tests were carried out in collaboration with Malvern Instrument d’Orsay (France) using a Mastersizer 3000 laser diffraction system equipped with an Aero S (Fig. 1a) to disperse the dry powders based on Mie’s theory. Plots of Fig. 1. b presents the particle size distribution of the PCMs dispersion.

The particle distribution of PCMs show a distribution as single-mode dispersion characterized by a single population centred at about 300 μm.

The morphology of the PCMs was observed using the Scanning Electron Microscope (SEM) technique. Observations were performed at room temperature. The SEM images have shown that most of the PCMs capsules exhibit quietly a spherical shape with different diameters. Some micrographs revealed that few of them presented broken shells probably due to the product handling or manufacture (Fig. 2).

2.2. PCM-concretes confection

In order to investigate the energy efficiency of the considered PCMs, different compositions of PCM-concrete were manufactured in laboratory with different proportions of PCMs (0%, 4.5%, 9%, 13%) by total mass of the cement. The dimensions of the specimen are $4 \times 4 \times 4$ cm^3 in order to enable the thermophysical characterization.

The formulation of the PCM-concretes was considered based on the previous research works of the authors [21,23,26].

Table 1 summarizes the composition of the manufactured mixtures.

Note that the PCM were added in the last stage of the manufacture process in order to avoid the capsules damage by shearing during concrete mixing [21,24].

The microstructure of PCM-concretes was observed by SEM technique as shown in Fig. 3. It was noted that introducing micro-encapsulated PCMs in the concrete matrix causes some microstructural changes through the presence of several pores of different size ranging from 1 mm to 50 mm as well as the presence of air bubbles.

In fact, the increase of porosity with the incorporation of micro-encapsulated PCM is mainly due to the formation of relatively larger crystalline products at the interface with the microencapsulated particles, which forms a more porous framework than in the mortar matrix (cement paste and sand particles). The larger the diameter of the microencapsulated PCM, the more pores will be in its interface with the

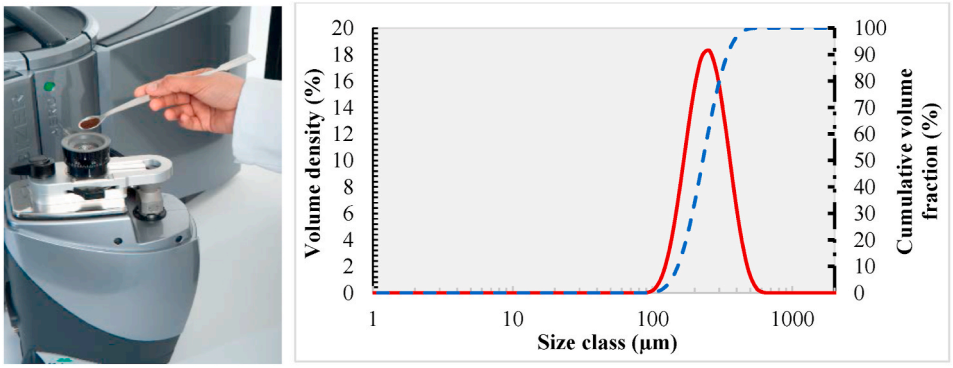

Fig. 1. (a) Dry process simpler Aero S, (b) Particle size curve of PCMs (continuous line), cumulative fractions (dashed line).

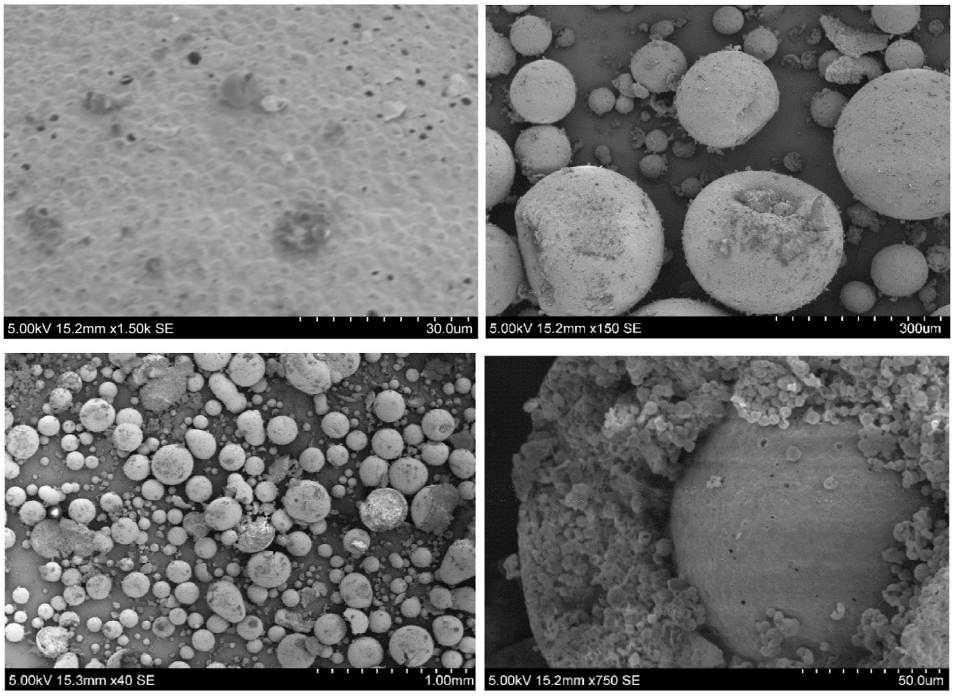

Fig. 2. SEM Observations of PCMs.

Table 1
PCM-concretes formulations.

	Cement (kg)	Aggregate (kg)	W/C (water to cement ratio)	PCMs (%)
PCM-concrete	360	1824	0.45	0, 4.5, 9, 13

cement mortar. These findings have been further discussed in an extensive previous research of the authors dealing with the porosity and the moisture transport properties investigation of the PCM-concrete. For more information, the reader could consult the research works of [27].

2.3. *Thermal analysis by DesProTherm*

In order to investigate the thermal behavior of the PCM-concrete, an original experimental setup was used. This bench test called "DesPro-Therm" was developed in laboratory and designed according to the certified ISO 9001 (version 2008).

The DesProTherm setup looks like hot plate setups commonly used for thermal properties measurements. The principle of the test consists on imposing a heat flux by a heating source to the tested specimen and then measuring the temperature evolution by thermo couples placed on the lower and upper surfaces of the specimen. The latter was isolated by placing a 4-cm thickness of insulation layer in contact with their lateral surfaces as shown in Fig. 4.

It shall be noted that tests were conducted 3 times for each case.

3. FEM numerical simulation

3.1. *Theoretical background*

The heat transfer phenomenon during PCM phase transition can be described by the Enthalpy Method [16]. The CFD software FLUENT uses a solidification-melting model based on this method, to solve the heat transfer problems during the solidification and melting processes.

Let recall that the energy transfer equation of the solid region in FLUENT is given as follows:

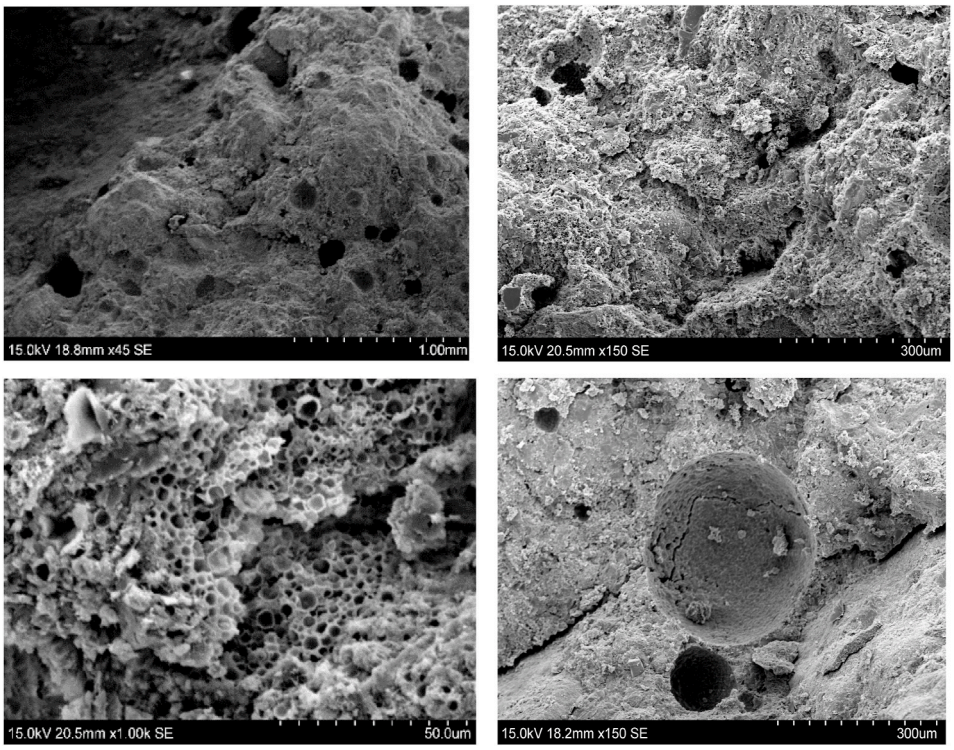

Fig. 3. SEM Observations of PCM-Concrete.

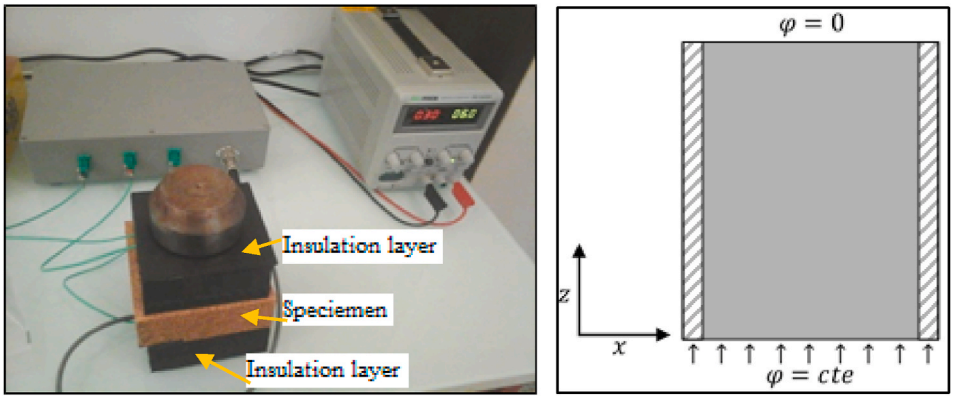

Fig. 4. Experimental setup (on the left), schematic representation (on the right).

$$\frac{\partial}{\partial t}(\rho h) + \nabla.(\vec{v}\rho h) = \nabla.(\lambda \nabla T) + S_h \quad [1]$$

Where:$\rho$is the density [kg.m^{-3}].

h is the sensible enthalpy [J]
$\vec{v}$ is fluid velocity (m.s^{-1})
$\lambda$is thermal conductivity [W.m^{-2}•K^{-1}]
T is temperature [K]
S_h is volumetric heat source [W.kg.m^{3}]

Note that the formula of the enthalpy H in the energy equation within the phase transition region is different from the enthalpy within the solid region. The former includes sensible enthalpy h and latent enthalpy. Accordingly, during the phase change, the enthalpy is given as:

$$H = h + \Delta H \quad [2]$$

Whereas the sensible enthalpy h is expressed as:

$$h = h_{ref} + \int_{T_{ref}}^{T} C_p dT \quad [3]$$

Where: h_{ref} is the reference enthalpy.

T_{ref} is the reference temperature,
C_p is the specific heat at constant pressure.

In order to calculate latent enthalpyΔH, the concept of liquid fraction$\beta$is introduced into the solidification-melting model of FLUENT [28], which is defined as follows:

$$\begin{cases} T < T_{solid} \\ T_{solids} < T < T_{liquid} \\ T > T_{liquid} \end{cases} ; \begin{matrix} \beta = 0 \\ \beta = \dfrac{T - T_{solid}}{T_{liquid} - T_{solid}} \\ \beta = 1 \end{matrix} \quad [4]$$

Where T_{solid} is the temperature at solid state [K],

T_{liquid} is the temperature at liquid state [K].

The latent heat content ΔH can now be written as:

$$\Delta H = \beta L \quad [5]$$

Where L is the latent heat of the material (unite). The latent heat content can vary between zero (for a solid) and L (for a liquid). For the solidification-melting process, the energy equation is written as:

$$\frac{\partial}{\partial t}(\rho H) + \nabla.(\vec{v}\rho H) = \nabla.(\lambda \nabla T) + S_h \quad [6]$$

The solution for temperature is essentially iteration between the energy equation and the liquid fraction equation.

3.2. Cases studies of PCM-wallboards

The wallboard of PCM-concrete considered in the numerical study has a height "H" of 3 m and a thickness "e" equal to 12 cm (Fig. 5). This thickness was considered based on the previous study of Cabeza et al. [4], where concrete cubicles were built with walls of 12 cm of thickness.

Numerical simulations were carried out using a CFD (Ansys/Fluent) calculation code. The PCM distributions in the wallboard can be described in different ways. In this study, three distributions were considered (Fig. 6):

Case 1. homogeneous wallboard of **PCM-concrete**, for this case, the equivalent effective properties are considered. The homogenized properties of PCM-concrete are presented in Table 3 (right column).

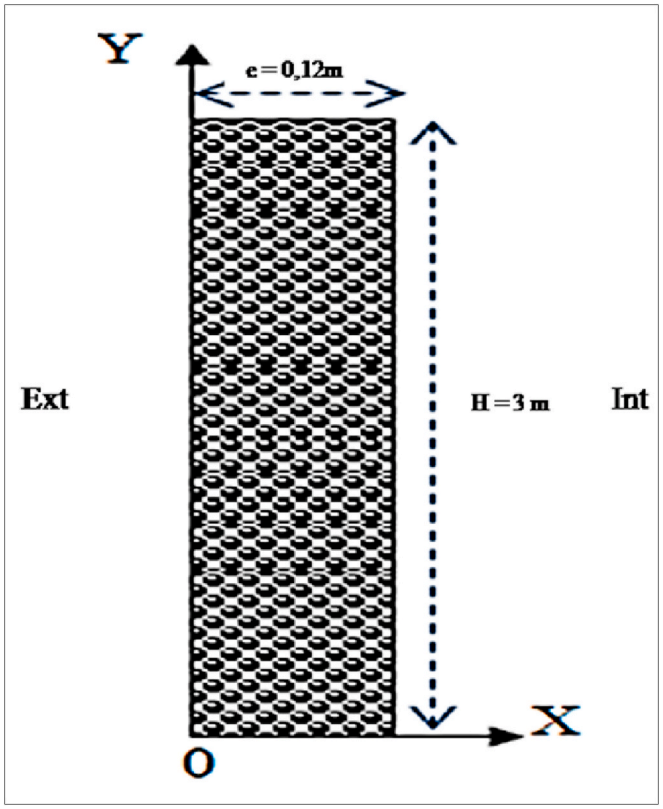

Fig. 5. Geometric characteristics of PCM Wallboard.

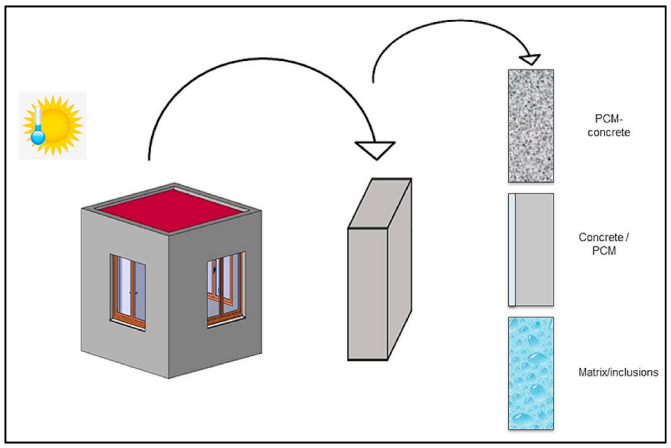

Fig. 6. Different cases studies of PCM-wallboards.

Case 2. bilayer wall: **Concrete/PCM**; the PCM layer is integrated on the exterior face of the wallboard (the PCM layer is supposed to have a thickness of 0.5 cm based on the previous study of the authors [27]). In this case, the thermophysical properties of PCMs (Table 2) and the Reference concrete (Table 3, left column) are considered separately.

Case 3. Concrete matrix incorporating PCM inclusions: **Matrix/inclusions**. Il this case, the thermophysical properties of PCMs (Table 2) are used for the inclusions whereas the properties of the Reference concrete (Table 3, left column) are attributed to the matrix.

In addition, an ordinary concrete wall, without PCM, was also considered as a reference for comparison with the three cases.

Note that for the numerical simulation, the proportion of PCMs in the PCM-concrete wallboard was taken equal to 4.5% by total mass of the cement. This value was previously retained by the authors [21,23] since it was demonstrated that this amount led to the best compromise between the thermal properties and the mechanical strength of the PCM-concrete.

Tables 2 and 3 present the thermophysical properties of PCMs, the reference concrete and PCM-concrete which will be used as data for the numerical simulation. The experimental data of bulk density, specific heat and thermal conductivity were gathered from the previous works of the authors [21].

3.3. Thermal scenarios

Different thermal scenarios were considered in this study as Neumann boundary conditions in order to take into account the various weather configurations. Note that the Dirichlet conditions are rarely encountered in the walls of a naturally functioning building. The different thermal scenarios are summarized in Fig. 7.

3.3.1. Scenario 1: $T_{int} = 19\ °C$; T_{ext} variable, $h_i = 4\ W\ m^{-2}\ K^{-1}$

In this case, the interior temperature was kept constant at 19 °C, while the exterior temperature is supposed following a sinusoidal temporal evolution:

$$T_{ext}(t) = 300 + 22\sin(\pi t) \quad [7]$$

Table 2
Thermophysical properties of PCMs.

	PCMs		
ρ [kg.m^{-3}]	1000		
T [°C]	**[5–20]**	**[20–30]**	**[30–50]**
Cp [J.kg^{-1}.K^{-1}]	2000	33000	2000
λ [W.m^{-1}.K^{-1}]	0.18		

Table 3
Thermophysical properties of reference and PCM-concrete.

	Reference Concrete			PCM-concrete		
ρ [kg.m^{-3}]	2375			2407		
T [°C]	**[5-20]**	**[20–30]**	**[30–50]**	**[5–20]**	**[20–30]**	**[30–50]**
Cp [J. kg^{-1}. K^{-1}]	561	627	671	699	933	699
λ[W.m^{-1}. K^{-1}]	2.01	1.97	1.94	1.93	1.74	1.61

The exchanges between the interior air and the wallboard were highlighted by an exchange coefficient ($h_i = 4$ W m^{-2} K^{-1}).

3.3.2. Scenario 2: *$T_{int} = 19$ °C; T_{ext} variable; $h_i = 4$ W m^{-2} K^{-1}; $h_e = 16$ W m^{-2} K^{-1}*

In this scenario, Neumann boundary conditions were considered on both vertical sides of the wallboard. The exchange with the adjacent environment are reflected on each side by equivalent exchange coefficients $h_i = 4$ Wm^{-2}K^{-1} and $h_e = 16$ Wm^{-2}.K^{-1}.

On the vertical side indoor, the temperature is taken equal to19°C, while the external temperature evolves sinusoidally:

$$T_{ext}(t) = 300 + 22\sin(\pi t) \quad [8]$$

3.3.3. Scenario 3: *T_{int} variable; $T_{ext} = 27$ °C; $h_i = 4$ W m^{-2} K^{-1}; $h_e = 16$ W m^{-2} K^{-1}*

In this configuration, the outside temperature of the wallboard was fixed to 27 °C while the interior temperature is sinusoidal:

$$T_{int}(t) = 292 + 12\sin(\pi t) \quad [9]$$

Note that the values of the exchange coefficients h_i and h_e were fixed based on the current values commonly used in buildings for France weather [29].

4. Results and discussion

4.1. Experimental results

This section presents the main results obtained by the DesProTherm experimental setup. The sampling frequency of readings was 0.1 s, and the readings were recorded continuously.

Fig. 8 shows the measured temperature over time on the lower (z = 0) and upper (z = e) surfaces of the control (0% PCM) and PCM-concrete specimens (4.5%, 9% and 13% PCM) with a thickness of 4 cm. Note that the tests was repeated 3 times and the maximal error recorded was less than 0.4°C.

It can be noted from plots of Fig. 8 that the different curves present the same tendencies as the temperature increases as a function of time. Besides, the two temperature curves on the upper and lower sides are looking to be quietly parallel which can be synonym of a similar thermal behavior of the PCM-wallboard on the upper and lower faces. The shift between the two curves is due to the fact that the heating element was positioned close to the lower face (z = 0) of the tested sample.

In order to discuss the effect of the PCM addition on the thermal behavior of the concrete, the temperature rise ΔT (°K) was computed of the upper face for concrete specimens for the different amounts of PCM considered in this study. The results are depicted in Fig. 9.

One can notice from plots of Fig. 9 that the temperature rise ΔT on the upper face decreases linearly with the addition of PCM as highlighted by the dashed interpolation line. The more PCMs are added in the concrete, the lower is the gradient of temperature in the specimen. For instance, it was recorded a loss of nearly 5%between the reference concrete and the "PCM-concrete 1" with 4.5% of PCMs. By analogy, losses of 12% and 17% were respectively noticed between the reference concrete and "PCM-concrete 2", on the one hand and "PCM-concrete 3", on the other one. This finding is very interesting since it emphasises on the main role of PCMs which consists not only on decreasing temperature but also on reducing thermal gradient in the material. By loosing some degrees of temperatures, the PCM look like a barrier which absorbs the exceed of calories in order to best maintain a stable thermal state

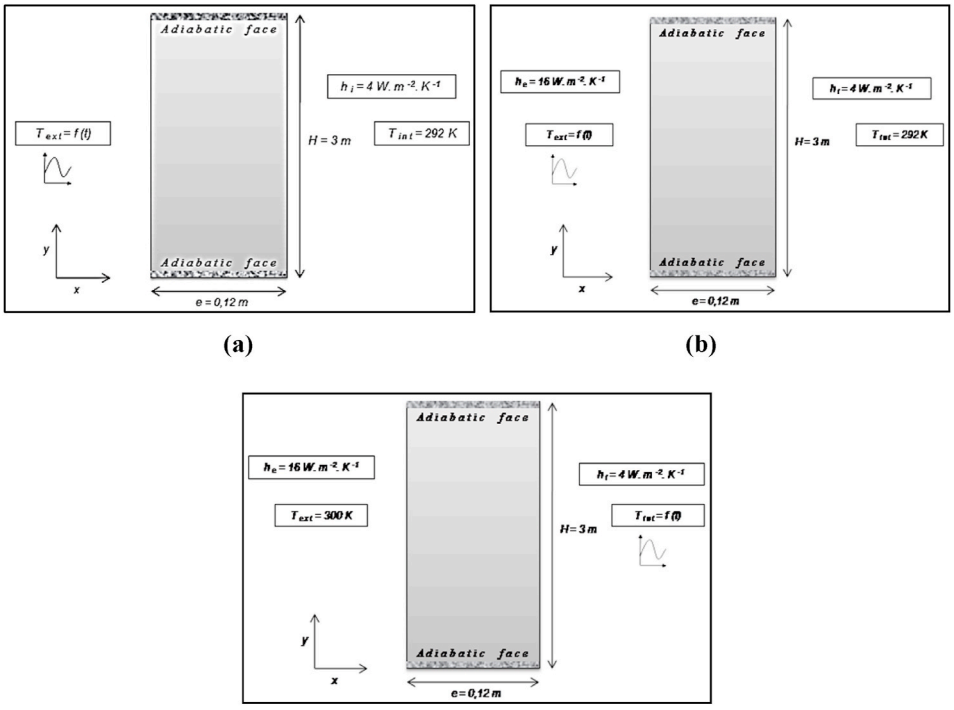

Fig. 7. Different thermal scenarios: (a) scenario 1, (b) scenario 2, (c) scenario 3.

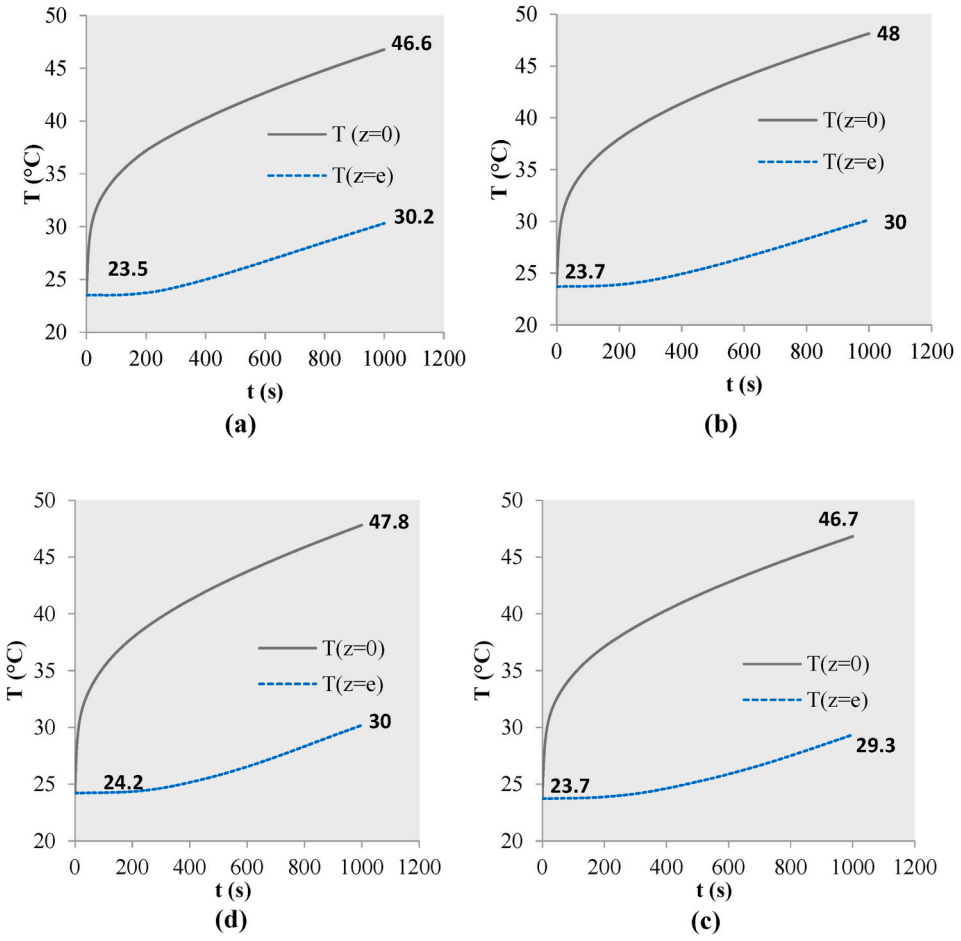

Fig. 8. Temperature evolutions recorded by the DesProTherm (PCM-concretes, e = 4 cm): (a) 0% PCM; (b) 4.5% PCM, (c) 9% PCM; and (d) 13% PCM.

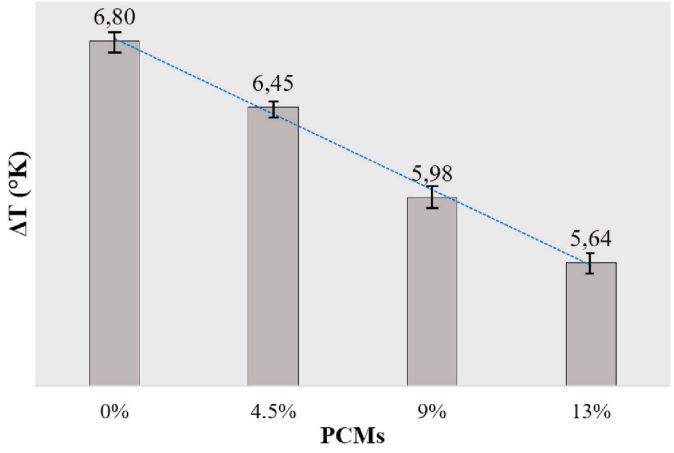

Fig. 9. Temperature rise ΔT (K) of the upper face for PCM-concrete.

with small fluctuations.

4.2. Numerical analysis

4.2.1. Model validation and confrontation with the experimental approach

Numerical simulation was also performed on the cube PCM-concrete of 4-cm of dimension in order to compare the results with the before mentioned experimental ones. It shall be noted that the data used for the numerical simulation are derived from the homogenized experimental results presented previously in Table 3. The numerical results are illustrated in Fig. 10.

Plots of Fig. 10 present the comparison between the thermograms obtained by the experimental and the numerical approaches. It can be noted that the numerical method presents an excellent agreement with the experiments. Furthermore, when comparing the time used for each approach, it appears that for this test, the simulation time was estimated to only 3 min whereas the experimental test, required at least 20–30 min to perform the experiment. Thus, it's clearly advantageous to use numerical tools in order to save time and a lot of experimental laboratory work.

In addition, and in order to better compare the experimental and numerical results, the results of the temperature gradient were gathered

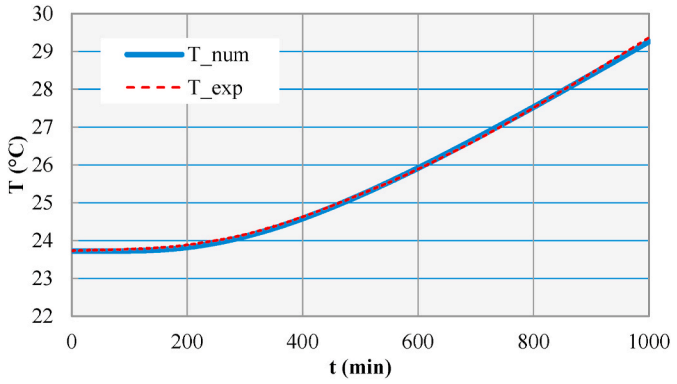

Fig. 10. Comparison between numerical and experimental temperature evolution results.

and computed for the different PCM-concrete mixtures. The results are summarized in Fig. 11. Once again, it can be noted that the numerical fluent model shows a good correlation with the experience results in terms of temperature gradient evolution. Based on these findings, the numerical model is validated and it will be used in the following, for the investigation of the thermal behavior of the PCM-concrete wallboard.

4.2.2. *Model generalization and analysis of the different scenarios*

In this section, the finite element numerical model was used and generalized for the simulation of the thermal behavior of the PCM-concrete wallboard described in Fig. 5. The results corresponding to the different thermal scenarios as well as the different PCM distributions in the wallboard are presented in the following.

4.2.2.1. Scenario 1: $T_{int} = 19\ °C$, T_{ext} variable, $h_i = 4\ W\ m^{-2}\ K^{-1}$. Fig. 12 shows the profile of the temperature evolution versus time for the different PCM-wallboards studied in the first scenario. Note that the PCMs have a melting temperature of 25 °C and a solidification temperature of 20 °C. The difference between the transition values can highlight a supercooling phenomenon. Therefore, the thermal disturbance appearing in the PCM-concrete wallboard can be justified by the phase change transition.

As can be seen, the curves exhibit a similar temperature profile for all the PCM-wallboards case studies, but with different extremums and time shifts. In fact, for the homogeneous wall of PCM-concrete (case study 1), the results of the simulation show that after 7h 27min, the maximum temperature reaches 32.3°C while that of the reference wall exceeds 33.1°C. Thus, the PCM allows a temperature decrease ΔT of about 0.8 °C and a time shift of 14 min during the storage phase. During the release phase, when PCMs are cooled, one notice that after 19h 36 min, the minimum temperature of the homogeneous wall of PCM-concrete reaches 19.6 °C while that of the reference wall 17.2 °C. Then, this configuration offers a temperature decrease ΔT of about 2.3 °C and a time shift of 28 min.

By analogy, the results of the simulation in the case of the bilayer wallboard PCM/concrete (case study 2) show that after 8h 24 min, the maximum temperature reaches 31.5°C while that of the reference wall exceeds 33.5°C. Accordingly, a temperature decrease of approximately 2 °C and a time shift of 56 min were recorded for this case during the storage phase. After 20 h 18 min, the temperature of the bilayer wall drops to 18.4 °C, while that of the reference wall decreases to 17.6 °C. Accordingly, a temperature decrease of approximately 0.8 °C and a time shift of 70 min were recorded for this case during the release phase.

Note that the PCM layer is supposed positioned on the exterior face of the wallboard. Naturally, the heat flux transits from the outside to the indoor across the wallboard. Because of the same outdoor environment conditions between the case studies 1 and 2, one can attribute the decrease of the surface temperature amplitude to the PCM layer which could played the role of a barrier for the heat, impeding thereby the temperature elevation inside the wall. On the other hand, the increase of time shift for Cases 1 and 2 in comparison with the reference concrete,

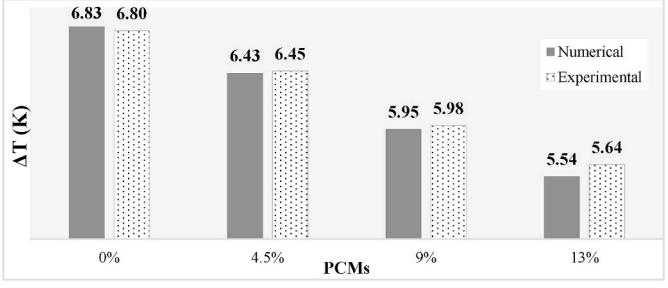

Fig. 11. Comparison between experimental and numerical Temperature gradient results.

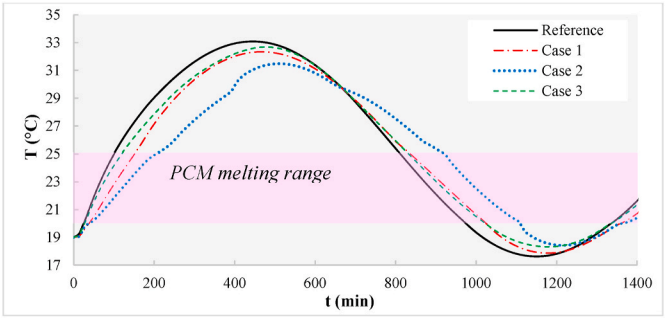

Fig. 12. Temperature evolution over 24 h for the different models studied (scenario 1).

highlighted that the PCMs can delay the heat transfer from outdoor to indoor space. These findings are more pronounced in the case of the bilayer wallboard for which the PCMs reinforcement at the front of the wallboard have led to better thermal performance.

The analysis of the case study 3 (Matrix/inclusions) for which the inclusions of PCMs are supposed embedded in the concrete matrix, one can note that the temperature evolution of the PCM-Concrete wallboard are close to the reference case. The difference between the temperatures reaches a maximum of 0.4 °C during the storage phase versus 0.7 °C when PCMs released. The time shift recorded was about 28 min between the two peaks. Thus, this case study of PCM-Concrete seems to exhibit a slight better thermal response than the reference concrete.

The different curves for the 4 wallboards show a hysteresis phenomenon: the temperature evolution starts the storage phase from the value of 19 °C but it ends the release phase with a temperature of 22 °C. This finding leads to the structure of a porous material, which has been proven by the authors in previous works [27].

Fig. 13 shows a comparison between the temperature profiles during the storage (Fig. 13a) and the release (Fig. 13b) periods for the different PCM wallboards.

We notice that between 42 min and 7h 28 min, the reference wall has the highest temperature. The peak deviation ΔT reaches a maximum value of 1.6 °C recorded in the case of the bilayer wallboard.

Table 4 summarizes the temperature differences and time shifts between the different PCM-wallboards for scenario 1.

Based on the aforementioned results, it can be concluded that, under the conditions indicated in this scenario, the bilayer wall exhibits the best thermal behavior in comparison with the other configurations since the PCM distribution was managed such as to ensure an insulation exterior layer. This result is interesting in the sense that the main objective of using PCMs is to improve thermal comfort inside the room by, among other things, limiting the temperature during periods of overheating.

4.2.2.2. Scenario 2: *$T_{int} = 19\ °C$; T_{ext} variable; $h_i = 4\ W\ m^{-2}\ K^{-1}$; $h_e = 16\ W\ m^{-2}\ K^{-1}$.* Fig. 14 shows the temperature evolutions versus time for the different PCM-wallboards studied in the second scenario.

It can be seen in the light of the temperature profile that for the hottest period of the day, the temperature of the PCM-concrete wallboard reaches 28°C in the case of homogeneous distribution, 26.6 °C for the bilayer wall and 29 °C in the case of a "Matrix/Inclusions" distribution, while the temperature in the reference concrete wall exceeds 29.5 °C. Thus, this configuration offers a temperature decrease ΔT of about 1.5 °C, 3 °C and 0.3 °C and a time shift of 70 min, 42 min and 28 min during the storage phase for the Homogeneous wall "Case 1", the Bilayer wall "Case 2", and the Matrix/Inclusions "Case 3", respectively.

The phenomenon is reversed overnight. In fact, the temperature of the PCM-concrete wallboard drops to 19.8 °C for the Homogeneous wall "Case 1", 19.2 °C for the Bilayer wall "Case 2", and 20 °C for the Matrix/Inclusions "Case 3", while that of the control wall returns to the initial

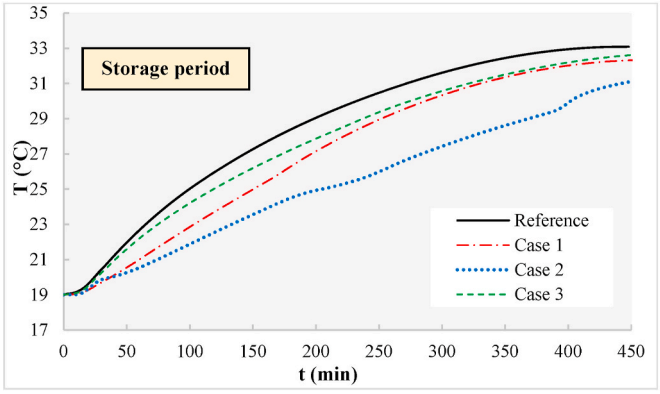

(a)

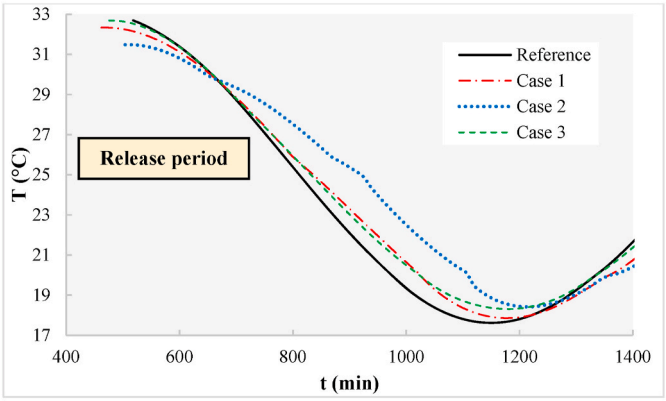

(b)

Fig. 13. Temperature evolution profiles (Scenario 1).

Table 4
Temperature gradient and time shift of the different PCM distributions (scenario 1).

	Storage phase		Release phase	
	ΔT (°C)	Time shift (min)	ΔT (°C)	Time shift (min)
Homogeneous wall "Case 1"	0,8	14	2.3	28
Bilayer wall "Case 2"	2	56	0,8	70
Matrix/Inclusions "Case 3"	0.4	28	0.7	28

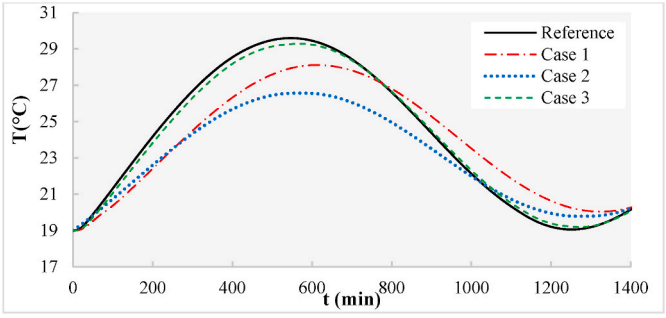

Fig. 14. Temperature evolution over 24 h for the different walls studied (scenario 2).

temperature (19 °C). Then, it was noticed a temperature decrease ΔT of about 1 °C, 0.7 °C and 0.1 °C and a time shift of 84 min, 42 min, and 28 min during the release phase for the Homogeneous wall "Case 1", the Bilayer wall "Case 2", and the Matrix/Inclusions "Case 3" respectively.

Table 5 presents the Temperature difference and time shift between the different walls for scenario 1.

In general, it can be noticed from the simulation results that the presence of PCMs leads to the decrease of both temperature peaks and fluctuations. However, in the case study 3, the temperature decrease was not significant. ΔT = 0.3 °C with a time shift of 28 min). This result can be attributed to the small quantity of PCM capsules in the wall (3%).

On the other hand, the homogeneous wall "Case 1" presents a good temperature decrease and a time shift during the two phases (storage and release) whereas the Bilayer wall "Case 2" shows an important drop of temperature ΔT = 3 °C during the storage phase, but this performance was limited during the release phase with ΔT estimated to 0.7 °C. During the two phases, the time shift was constant and equal to 42 min.

In any case, the energy efficiency of PCM wallboards was enhanced compared with the reference one, but once again the case study 2 can be distinguished by a better thermal performance comparing to the Cases 1 and 3.

4.2.2.3. Scenario 3: *T_{int} variable; T_{ext} = 27 °C; h_i = 4 W m^{-2} K^{-1}; h_e = 16 W m^{-2} K^{-1}.* Fig. 15 shows the temperature evolution under time on the different walls studied in the third scenario.

The analysis of the above results shows that for the case of a homogeneous distribution "Case 1", the maximum temperature reaches 26.3 °C after 9 h 6 min, while the maximum temperature of the reference wall is 27.2 °C after about 8 h 24 min. It was recorded a time shift of 42 min and a temperature gradient of 0.9 °C during the storage period.

For the Bilayer wallboard "Case 2", the temperature exhibits a variation from 19 °C to 25.6 °C while the temperature of the reference wall varies from 19°C to 27.2 °C. Moreover, the maximum peak of the temperature in the bilayer wall appears with a delay of 1h and 24 min compared to that of an ordinary wall, which means that the thermal inertia of the PCM-concrete was enhanced.

The placement of the PCM layer helps to maintain a certain level of comfort in the room with a resulting temperature evolving sinusoidally above the initial temperature. Also, it can be seen that the temperature does not increase significantly above the melting point of PCMs (26 °C).

For the case study 3 with a Matrix/Inclusions distribution, we notice that the temperature presents a general appearance similar to that of the reference wall except during periods of low exchanges (at the end of the release period), where significant differences between the two walls can be observed. It was recorded a maximum temperature of 27.2 °C after 8 h and 24 min for the concrete wall while it reaches only 26 °C after 8 h and 38 min for the Microcapsules PCM-Concrete wall.

Table 6 presents the Temperature difference and time shift between the different walls for scenario 3.

We note that the bilayer wall presents the best performances: an important decrease in the temperature fluctuations (ΔT = 1.6 °C) and a time shift of 1h 24 min and 42 min respectively between maximum and minimum temperatures reached compared to the reference wall.

Table 5
Temperature gradient and time shift of the different PCM distributions (scenario 2).

	Storage phase		Release phase	
	ΔT (°C)	Time shift (min)	ΔT (°C)	Time shift (min)
Homogeneous wall "Case 1"	1.5	70	1	84
Bilayer wall "Case 2"	3.0	42	0.7	42
Matrix/Inclusions "Case 3"	0.3	28	0.1	28

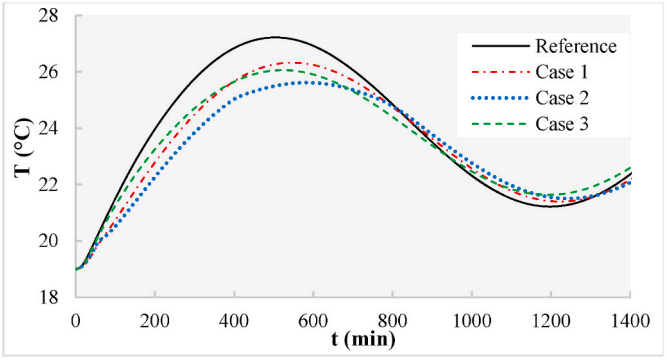

Fig. 15. Temperature evolution over 24 h for the different walls studied (scenario 3).

Table 6
Temperature gradient and time shift of the different PCM distributions (scenario 3).

	Storage phase		Release phase	
	ΔT (°C)	Time shift (min)	ΔT (°C)	Time shift (min)
Homogeneous wall "Case 1"	0.9	42	0.2	14
Bilayer wall "Case 2"	1.6	84	0.3	42
Matrix/Inclusions "Case 3"	1.2	14	0.4	14

It shall be noted that the performance of the matrix/inclusions wall (Case 3) in comparison with the homogeneous wall (Case 1) in the scenario 3, could be attributed to the fact that in this scenario, the interior temperature is variable in contrast with the previous scenarios 1 and 2, however external temperature is constant. Accordingly, the thermal fluctuations are not very high. Thus, the presence of the microencapsulated PCMs dispersed in the concrete matrix is enough to attenuate those fluctuations.

5. Conclusions

In this work, a finite element numerical method was used for the thermal simulation of concrete wallboards impregnated with phase change materials. Based on the experimental measurements of the temperature evolution, derived from a DesProTherm original setup developed in laboratory, this method allows the simulation of the thermal response of a PCM-concrete wallboard under different climate configurations. The comparison of the Data with the numerical findings have shown a good correlation in terms of the temperature evolution results. This allows the validation of the numerical tool and its generalization to the case of PCM-concrete full-scale wallboards.

Furthermore, the analysis of the results gathered from the different cases of PCM distributions highlighted an enhancement of the thermal inertia of the PCM-wallboard and a better energy efficiency especially in the case of a bilayer configuration (PCM/concrete). This finding can be explained by the presence of a pure PCM layer which could have played the role of a barrier absorbing the heat excess and delaying the temperature peak to later time. The time delay can be synonym of the energy efficiency of the used PCMs since the shift of the temperature peak to later times can imply a less use of the air-conditioning systems by the occupants and lead accordingly to economic and environmental benefits. Besides, it shall be noted that a better energy efficiency of PCMs could have been ensured if the PCM layer was thicker than the studied case of 0.5 cm since the thermal inertia and heat storage capacity of PCM layer are higher than those of concrete.

For all the studied scenarios, the numerical developed tool has shown its reliability to offer a fast prediction of the thermal response of PCM wallboards, saving thereby a heavy experimental campaign. This tool can also be used to achieve simulations with more severe conditions based on several international climates.

Work is now undertaken in laboratory to experimentally investigate the thermal efficiency of the PCM-concrete wallboards equipped with a monitoring system in order to study their behavior under real weather conditions. In future, it would also be interesting to generalize the numerical developed tool to the case of a full-scale test cell with PCMs in order to improve our understanding about the effective contribution of PCMs at the building scale.

Author agreement statement

I declare that this manuscript is original, has not been published before and is not currently being considered for publication elsewhere.

I confirm that the manuscript has been read and approved by all named authors and that there are no other persons who satisfied the criteria for authorship but are not listed.

I further confirm that the order of authors listed in the manuscript has been approved by all of them.

I understand that the Corresponding Author is the sole contact for the Editorial process. She is responsible for communicating with the other authors about progress, submissions of revisions and final approval of proofs Signed by all authors.

Declaration of competing interest

The authors declare that they have no known competing financial interests or personal relationships that could have appeared to influence the work reported in this paper.

References

[1] J. Lei, J. Yang, Energy performance of building envelopes integrated with phase change materials for cooling load reduction in tropical Singapore, Appl. Energy 162 (2015) 207–217.
[2] E. Asadi, M.G. Da Silva, C.H. Antunes, L. Dias, Multi-objective optimization for building retrofit strategies: a model and an application, Energy Build. 44 (2012) 81–87.
[3] L.F. Cabeza, A. Castell, C. Barreneche, A. De Gracia, A.I. Fernández, Materials used as PCM in thermal energy storage in buildings: a review, Renew. Sustain. Energy Rev. 15 (3) (2011) 1675–1695.
[4] L.F. Cabeza, C. Castellon, M. Nogués, M. Medrano, R. Leppers, O. Zubillaga, Use of microencapsulated PCM in concrete walls for energy savings, Energy Build. 39 (2) (2007) 113–119.
[5] B. Zalba, , J.M. Marín, L.F. Cabeza, H. Mehling, Review on thermal energy storage with phase change: materials, heat transfer analysis and applications, Appl. Therm. Eng. 23 (3) (2003) 251–283.
[6] M. Hunger, A.G. Entrop, I. Mandilaras, H.J.H. Brouwers, M. Founti, The behavior of self-compacting concrete containing micro-encapsulated Phase Change Materials, Cement Concr. Compos. 31 (10) (2009) 731–743.
[7] A. M. Khudhair, M. M. Farid, A review on energy conservation in building applications with thermal storage by latent heat using phase change materials, Energy Convers. Manag.. 45(2) ( ) 263-275.
[8] A. De Gracia, L. Navarro, A. Castell, A. Ruiz-Pardo, S. Alvárez, L.F. Cabeza, Experimental study of a ventilated facade with PCM during winter period, Energy Build. 58 (2012) 324–332.
[9] Z.I. Djamai, F. Salvatore, A. Si Larbi, G. Cai, M. El Mankibi, Multiphysics analysis of effects of encapsulated phase change materials (PCMs) in cement mortars, Cement Concr. Res. 119 (2019) 51–63.
[10] P. Meshgin, Y. Xi, Multi-scale composite models for the effective thermal conductivity of PCM-concrete, Construct. Build. Mater. 48 (2013) 371–378.
[11] N. Soares, J. Costa, A.R. Gaspar, P. Santos, Review of passive PCM latent heat thermal energy storage systems towards buildings' energy efficiency, Energy Build. 59 (2013) 82–103.
[12] F. Mehdaoui, M. Hazami, H. Taghouti, M. Noro, R. Lazzarin, A. Guizani, An experimental and a numerical analysis of the dynamic behavior of PCM-27 included inside a vertical enclosure: application in space heating purposes, Int. J. Therm. Sci. 133 (2018) 252–265.
[13] D. Li, Y. Zheng, C. Liu, G. Wu, Numerical analysis on thermal performance of roof contained PCM of a single residential building, Energy Convers. Manag. 100 (2015) 147–156.
[14] P. Tittelein, S. Gibout, E. Franquet, K. Johannes, L. Zalewski, F. Kuznik, D. David, Simulation of the thermal and energy behaviour of a composite material containing

encapsulated-PCM: influence of the thermodynamical modelling, Appl. Energy 140 (2015) 269–274.
[15] J.S. Kim, K. Darkwa, Simulation of an integrated PCM-wallboard system, Int. J. Energy Res. 27 (3) (2003) 215–223.
[16] S. Karthikeyan, R. Velraj, Numerical investigation of packed bed storage unit filled with PCM encapsulated spherical containers – a comparison between various mathematical models, Int. J. Therm. Sci. 60 (2012) 153–160.
[17] J. Xamán, A. Rodriguez-Ake, I. Zavala-Guillén, I. Hernández-Pérez, J. Arce, D. Sauceda, Thermal performance analysis of a roof with a PCM-layer under Mexican weather conditions, Renew. Energy 149 (2019) 773–785.
[18] J. Yu, K. Leng, H. Ye, X. Xu, Y. Luo, J. Wang, W. Gang, Study on thermal insulation characteristics and optimized design of pipe-embedded ventilation roof with outer-layer shape-stabilized PCM in different climate zones, Renew. Energy 147 (2020) 1609–1622.
[19] M. Kheradmand, M. Azenha, J.L.B. de Aguiar, J. Castro-Gomes, Experimental and numerical studies of hybrid PCM embedded in plastering mortar for enhanced thermal behaviour of buildings, Energy 94 (2016) 250–261.
[20] Technical Information Sheet, Micronal DS 5038 X, BASF, the Chemical Company.
[21] S. Drissi, Development of New Concrete Energy Accumulator: Experimental, Probabilistic and Numerical Study of its Thermal Behavior, University Paris-Est, ENIT-Tunis, 2015. https://pastel.archives-ouvertes.fr/tel-01271597.
[22] N. Essid, A. Eddhahak, J. Neji, Experimental and numerical thermal properties investigation of cement-based materials modified with PCM for building construction use, J. Architect. Eng. 26 (3) (2020).
[23] A. Eddhahak, S. Drissi, J. Colin, J. Neji, Analysis by Differential Scanning Calorimetry of concrete modified with microencapsulated phase change materials, International Renewable and Sustainable Energy Conference (IRSEC) (2013) 337–342.
[24] A. Eddhahak, S. Drissi, J. Colin, S. Caré, J. Neji, Effect of phase change materials on the hydration reaction and kinetic of PCM-mortars, J. Therm. Anal. Calorim. 117 (2) (2014) 537–545.
[25] S. Drissi, A. Eddhahak, S. Caré, J. Neji, Thermal analysis by DSC of Phase Change Materials, study of the damage effect, Journal of Building Engineering 1 (2015) 13–19.
[26] A. Eddhahak-Ouni, S. Drissi, J. Colin, J. Neji, S. Care, Experimental and multi-scale analysis of the thermal properties of Portland cement concretes embedded with microencapsulated Phase Change Materials (PCMs), Appl. Therm. Eng. 64 (1–2) (2014) 32–39.
[27] N. Essid, A. Loulizi, J. Neji, Compressive strength and hygric properties of concretes incorporating microencapsulated phase change material, Construct. Build. Mater. 222 (2019) 254–262.
[28] V.R. Voller, M. Cross, N.C. Markatos, An enthalpy method for convection/diffusion phase change, Int. J. Numer. Methods Eng. 24 (1) (1987) 271–284.
[29] New Active Components for Thermal Management of the Light Envelope of Buildings. Coupling Phase Change Materials, Super-insulation, Solar Energy. Grenoble, 2004. https://www.theses.fr/2004GRE10167.